Vertical cross-spectral phases in atmospheric flow

A Chougule, J Mann and M Kelly
DTU Wind Energy, Risø Campus, 4000 Roskilde, Denmark
E-mail: absch@dtu.dk

Abstract. The cross-spectral phases between velocity components at two heights are analyzed from observations at the Høvsøre test site under diabatic conditions. These phases represent the degree to which turbulence sensed at one height leads (or lags) in time the turbulence sensed at the other height. The phase angle of the cross-wind component is observed to be significantly greater than the phase for the along-wind component, which in turn is greater than the phase for the vertical component. The cross-wind and along-wind phases increase with stream-wise wavenumber and vertical separation distance, but there is no significant change in the phase angle of vertical velocity. The phase angles for all atmospheric stabilities show similar order in phasing. The phase angles from the Høvsøre observations under neutral condition are compared with a rapid distortion theory model which show similar order in phase shift.

1. Introduction

The structure of atmospheric turbulence can be analysed in terms of two-point statistics such as normalized cross-spectra (also known as coherences), which are typically studied both experimentally and theoretically as a function of horizontal separation distance for homogeneous turbulence in the atmospheric surface-layer [1, 2]. The coherences of the along-wind, cross-wind and vertical velocity components (u, v, w) decrease with increasing separation distance, as seen from both observations and theory [2].

In this paper we investigate cross-spectra with particular emphasis on the associated phases φ for vertical separations Δz, using observations at Høvsøre under diabatic conditions [3, 4]. Chougule et al. [5] studied the vertical phase angles for all three velocity components (i.e. φ_u, φ_v and φ_w), including their behavior in the neutral, horizontally homogeneous atmospheric boundary layer (ABL) using measurement from Høvsøre and Cooperative Atmosphere-Surface Exchange Study in 1999 (CASES-99) [6, 7]. Mann [2] studied φ_{vw} (the phase angle between v and w) for horizontal separations, and $\varphi_{uu}(\equiv \varphi_u)$ and φ_{uw} for vertical separations where the w-component was measured further from the surface. Few experimental investigations have been done on the phases. Heidrick et al. [8] experimentally studied the phases of the axial velocity component in fully developed pipe flow using measurements taken at two different points, where the separation vector was oriented at different angles to the mean flow. Komori et al. [9] studied the phase angle between the vertical velocity-component and temperature in stably-stratified open-channel flow. Both Heidrick et al. [8] and Komori et al. [9] assumed turbulent motions approach as wavelike motions. The Sandia (Veers) method [10], which is used in wind engineering for load calculations on wind turbines, assumes an average of zero phase between any two points because of an exponential form of the coherence function as given in Ref. [11]. The Mann method [12], based on the Mann spectral tensor model [2] and widely used in wind

engineering, does give non-zero phases.

In addition to the observations, we also evaluate the phase angles from the Mann spectral tensor model [2] which incorporates rapid distortion theory (RDT) [13, 14]. The phases are determined by calculating the two-point cross-spectra of velocity components and corresponding spectra as defined in Section 1.2. The observations and the model used for the analysis are described in Section 2 and Section 3, respectively. The results from the observations and the RDT model are given in Section 4. In Section 5, we discuss more details, followed by conclusions in Section 6.

1.1. Motivation

Mann [2] modeled the evolution of turbulence induced by uniform shear using RDT [14, 13] in a neutral surface-layer. Mann [12] used the model of [2] to develop a method to simulate the three-dimensional wind in the time domain. The model in [2] and the method in [12] are the industry standards for aero-elastic calculation of wind turbine loads [15]. Turbulence simulations from [12] show systematic behavior in u, v and w fluctuations in the rotor plane of a horizontal axis wind turbine, and when used to predict the respective phase angles between two heights, we see that $\varphi_v > \varphi_u > \varphi_w$ for $k_1 \Delta z \leq 1$, where k_1 is stream-wise wavenumber. We expect that this behaviour in phasing is due to the vertical shear as depicted in Figure 1.

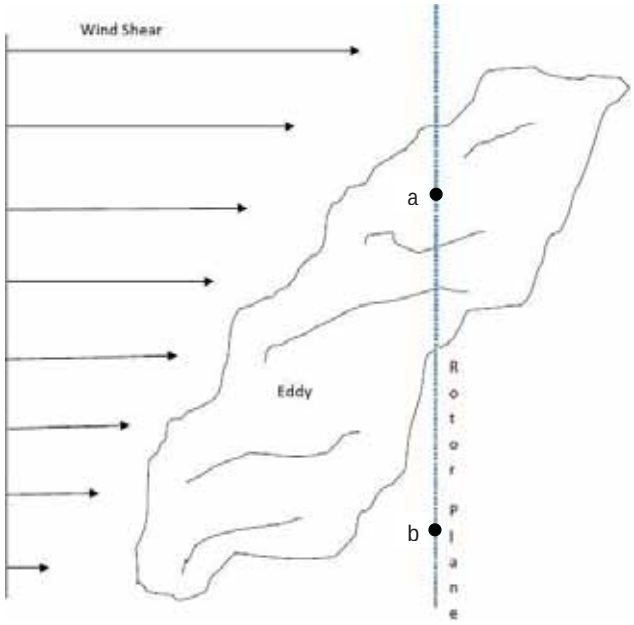

Figure 1. Sketch of the eddy stretching due to the shear. The turbulence sensed at point **a** leads in phase with respect to the turbulence sensed at point **b** in the rotor plane of a horizontal axis turbine.

Chougule et al. [5] shown that under neutral, horizontally homogeneous ABL, $\varphi_v > \varphi_u > \varphi_w$ and the RDT and LES modeled phases are consistent with the observed phases under neutral condition. There are two basic assumptions considered in the study of Chougule et al. [5], one neutral stratification and second horizontally homogeneous flow. In order to confirm in more detail about the phase shift due to the shearing effect and the phase behavior, we analyze diabatic data from Høvsøre with the essentially inhomogeneous flow.

1.2. Definitions

The phases are calculated from complex cross-spectra. The cross-spectrum between velocity components $u_i(t)$ $(i = 1, 2, 3)$ and $u_j(t)$ $(j = 1, 2, 3)$ at heights z_1 and z_2, respectively, is defined as

$$\chi_{ij}(f, \Delta z) = \langle \hat{u}_i(f, z_1) \hat{u}_j^*(f, z_2) \rangle, \tag{1}$$

where f is frequency, $\Delta z = z_2 - z_1$, $\langle\ \rangle$ denotes ensemble averaging, $*$ denotes complex conjugate and $\hat{u}_i(f, z_1)$ is the complex-valued Fourier transform of the i^{th} velocity component $u_i(t)$ at height z_1. The phase between the two velocity components is then

$$\varphi_{ij}(f, \Delta z) = \arg(\chi_{ij}(f, \Delta z)). \tag{2}$$

The coherences, sometimes known as "squared coherences", are calculated from the cross-spectra and the single-point power-spectra via

$$\mathrm{coh}_{ij}(f, \Delta z) = \frac{|\chi_{ij}(f, \Delta z)|^2}{F_i(f, z_1)F_j(f, z_2)}, \tag{3}$$

where $F_i(f, z) = \langle \hat{u}_i(f)\hat{u}_i^*(f) \rangle$ is the single-point power-spectrum of the i^{th} velocity component $u_i(t)$ at height z.

If we assume that Taylor's hypothesis of "frozen turbulence" is valid, then the measured time series can be related to spatial fluctuations. So for the stream-wise direction, single-point measurements can be related through $k_1 = 2\pi f/U$, where U is the stream-wise mean wind speed.

2. Høvsøre

The measurements are taken from the 116.5 m tall mast at the Høvsøre test site on the west coast of Denmark. Sonic anemometers, sampling at 20 Hz and measuring in three dimensions, are installed on the mast at heights of 10, 20, 40, 60, 80 and 100 m. The land to the east of the mast can be considered as flat, homogeneous terrain. On the west side of the mast, land extends 1500 m to the North Sea coast, including a dune which can affect the flow. Five wind turbines are situated to the north of the mast. More details about the location and instrumentation can be found in Refs. [3, 4].

Winds are selected from directions between 240° and 300° from where the flow is essentially inhomogeneous and the data limited to when the 80 m mean wind speeds fall between 8 and 9 m s^{-1}. The calculations are done for diabatic conditions, where atmospheric stability is classified based on the range of Obukhov lengths L_0 as given in Table 1 following [16]. The height interval chosen in the phase analysis spans 40 – 100 m. Analysis is done using seven years of data from 2004 to 2010.

Table 1. Classification of ABL into seven atmospheric stabilities following [16].

Obukhov Length (m)	Atmospheric Stability
$-100 \leq L \leq -50$	Very Unstable (VU)
$-200 \leq L \leq -100$	Unstable (U)
$-500 \leq L \leq -200$	Near Unstable (NU)
$\lvert L\rvert \geq 500$	Neutral (N)
$200 \leq L \leq 500$	Near Stable (NS)
$50 \leq L \leq 200$	Stable (S)
$10 \leq L \leq 50$	Very Stable (VS)

The Figure 2 show the probability of occurrences of different atmospheric stabilities from very unstable (negative L_o) to very stable (positive L_o) case. The Obukhov length L_o is defined

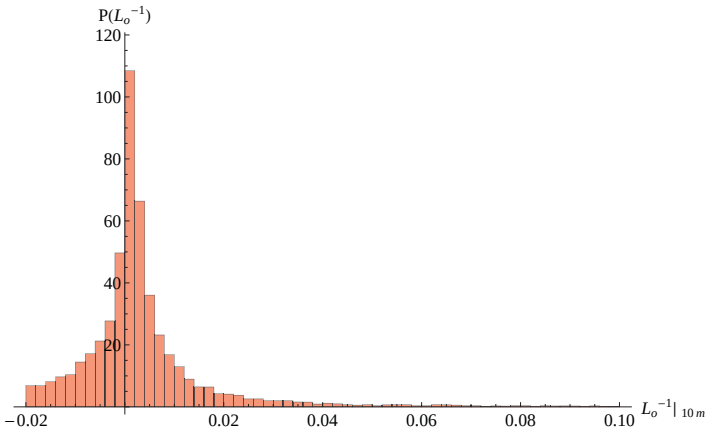

Figure 2. Histogram of atmospheric stabilities based on Obukhov lengths for wind directions between 240° and 300° at Høvsøre test site in the west coast of Denmark. ABL is classified into 7 stabilities following [16].

as

$$L_o = \frac{-{u_*}^3}{\kappa(g/T)\overline{w'T'}_0}, \tag{4}$$

where u_* is the surface friction velocity which is constant within the surface layer and decrease with the height above the surface layer, κ is the von Kármán constant (typically the value 0.4 is used), g is the acceleration due to gravity, T is the reference temperature (if moisture is included then T is the virtual temperature and due to conserved scalar, T becomes virtual potential temperature), $\overline{w'T'}_0$ is the virtual potential temperature flux at the surface.

3. Spectral tensor model

The Mann spectral velocity tensor model incorporates RDT [13, 14] with an assumption of a mean uniform shear, plus a wavenumber-dependent eddy lifetime, to estimate the structure of turbulence over uniform flat terrain, which has been extended to cover gently varying orography [18]. The model calculates the evolution of turbulence in Fourier modes from an initial isotropic state, the energy spectrum of which is given by the von Kármán form [19].

The Mann model contains three adjustable parameters:

- A length scale L describing the size of energy-containing eddies
- A non-dimensional anisotropy parameter Γ used in the parameterisation of the eddy lifetime
- A measure of the energy dissipation $\alpha\epsilon^{2/3}$, where the Kolmogorov constant $\alpha = 1.7$ and ϵ is the rate of viscous dissipation of specific turbulent kinetic energy.

The analytical form of the spectral velocity tensor in [2] is a function of these three parameters and can be expressed as $\Phi_{ij}(\boldsymbol{k}, L, \Gamma, \alpha\epsilon^{2/3})$, where $\boldsymbol{k} = (k_1, k_2, k_3)$ is the three-dimensional wave vector. The modeled cross-spectra which also become functions of the three parameters, are given as

$$\chi_{ij}(k_1, L, \Gamma, \alpha\epsilon^{2/3}, \Delta y, \Delta z) = \int \Phi_{ij}(\boldsymbol{k}, L, \Gamma, \alpha\epsilon^{2/3}) \exp(\mathrm{i}(k_2\Delta y + k_3\Delta z))\mathrm{d}\boldsymbol{k}_\perp, \tag{5}$$

where $\int \mathrm{d}\boldsymbol{k}_\perp \equiv \int_{-\infty}^{\infty}\int_{-\infty}^{\infty}\mathrm{d}k_2\mathrm{d}k_3$ and Δy is the transverse separation distance. The three parameters are determined by fitting model single-point power-spectra $F_i(k_1, L, \Gamma, \alpha\epsilon^{2/3}) = \chi_{ii}(k_1, L, \Gamma, \alpha\epsilon^{2/3}, 0, 0)$ (no summation), to the measured single-point power-spectra through chi-squared fitting as given in Ref. [2].

Figure 3 gives an example of a model fit of power-spectra to the Høvsøre data at 40 m height for unstable, neutral and stable conditions illustrating extraction of L, Γ and $\alpha\epsilon^{2/3}$. However,

the Mann spectral tensor model assumes neutral stratification, and the three parameters for non-neutral conditions can be obtained by forcing the model to fit with measured spectra through chi-squared fit [2]. The three parameters subsequently used as an input to calculate numerically the cross-spectrum between any two velocity components through equation (5). Thus for vertical separations ($\Delta y = 0$), the model cross-spectra and phases are expressed as $\chi_{ij}(k_1, L, \Gamma, \alpha\epsilon^{2/3}, \Delta z)$ and $\varphi_{ij}(k_1, L, \Gamma, \Delta z)$, respectively. The model phases are unaffected by ϵ.

The distortion of the wave vector due to shear $\mathrm{d}U/\mathrm{d}z$ is given by $\boldsymbol{k}(t) = (k_1, k_2, k_{30} - k_1(\mathrm{d}U/\mathrm{d}z)t)$, with the initial wave vector $\boldsymbol{k}_0 = (k_1, k_2, k_{30})$. The model assumes a uniform shear so $\mathrm{d}U/\mathrm{d}z$ is constant with height which is an approximation, but we do not expect that a non-zero $\mathrm{d}^2U/\mathrm{d}z^2$ would significantly alter the results. In addition to the uniform shear, the vertically inhomogeneous effect of blocking due to the surface (e.g. ground) was included in [2]; however, it does not produce significantly different results. Nevertheless, as discussed above, χ_{ij}, F_i and φ_{ij} are functions of L, which itself depends on the distance z from the ground. In this way the model treats vertical inhomogeneity in application.

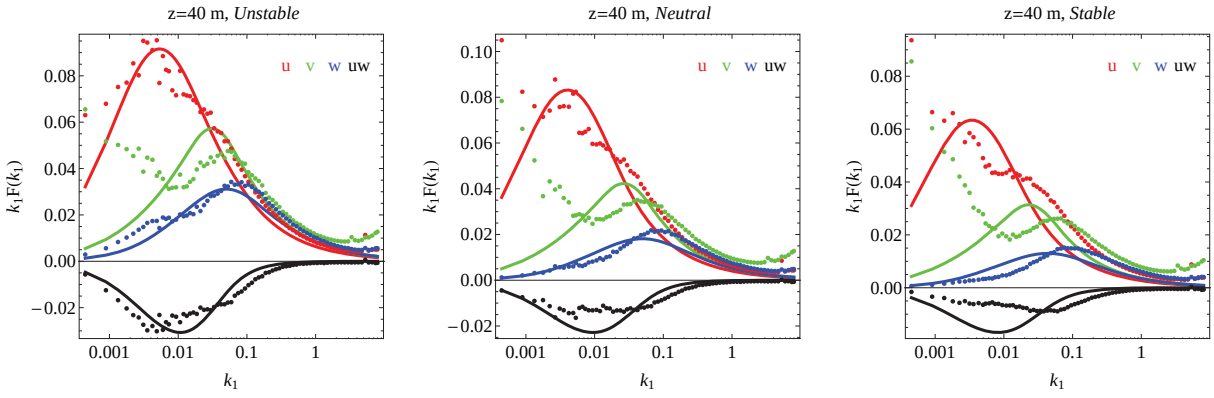

Figure 3. Example of the model fit of single-point spectra to the Høvsøre data at 40 m height to determine the three parameters in the Mann model [2]. Measured (co) spectra are denoted by points and smooth lines show modeled (co) spectra. Number of thirty-minute time series used: Unstable; 165, Neutral; 176 and Stable; 538.

In the next section, the results from the observations and the models are provided, followed by discussion in Section 5.

4. Results

The phases from the Høvsøre observations are shown in Figure 4(a) and the coherences in Figure 4(b), along with the predictions from the Mann model for neutral ABL. As described in Section 3.1, the three adjustable parameters in the model are determined by fitting the one-dimensional power-spectra of the model to that from the data at heights 40 and 100 m (see Figure 3). The average of the parameters at the two heights is used to calculate the model cross-spectra. The slopes of the phase curves predicted by the model are different than those calculated from the measurements. However, the model is able to predict the order in phasing, $\varphi_v > \varphi_u > \varphi_w$, for $k_1\Delta z \leq 1$.

The model overestimates the u-, v- and w-coherence for $k_1\Delta z \leq 1$. So at a given length scale, the fluctuations at two corresponding heights in the modeled coherent eddies are more correlated than those from the observation. It is also observed that the modeled phases are smaller than the phase angles from the measurements.

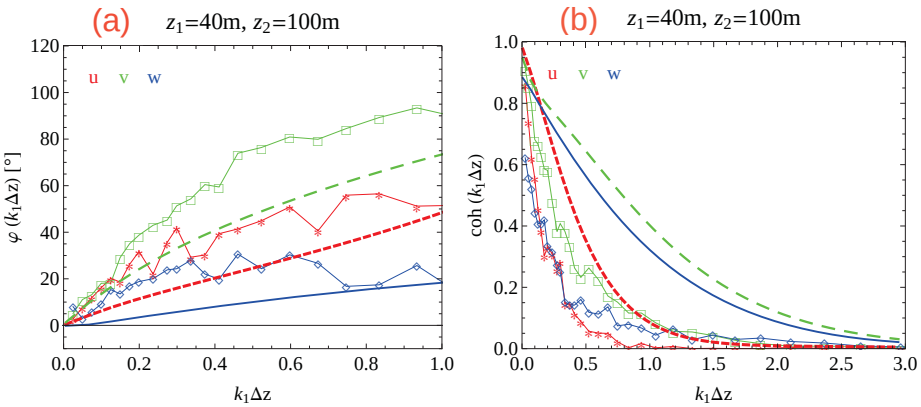

Figure 4. The phases (a) and the coherences (b) between 40 and 100 m at Høvsøre for a neutral ABL fitted with the Mann model [2]. Measurements: φ_u; –∗–, φ_v; –□–, φ_w; –◇–. Model: φ_u; **- - -**, φ_v; – – –, φ_w; ——. Similar notations are followed for the coherences.

When phases are examined with different atmospheric stabilities, we observe same order in phase shift for three velocity components as depicted in Figure 5.

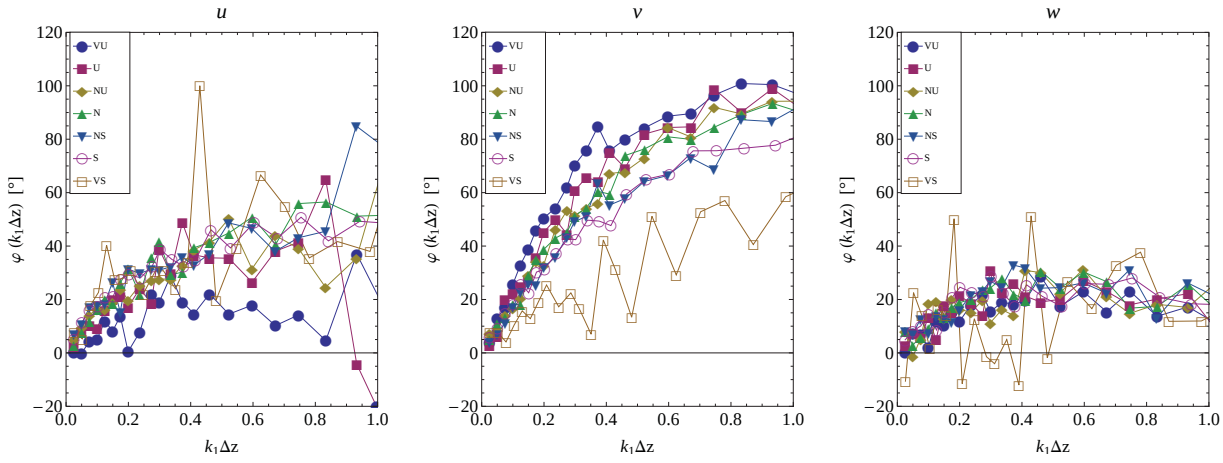

Figure 5. The phases between 40 and 100 m at Høvsøre for different atmospheric stabilities for wind directions between 240° and 300°. Atmospheric stability is classified into seven stabilities (very unstable to very stable) following [16].

5. Discussion

In this section we describe some more details about the behaviour of the phases under diabatic conditions. The phase angles for neutral ABL are studied and compared with the RDT and LES model in Chougule el al. [5], where the winds at Høvsøre are selected from east (between 60° and 120°) with essentially homogeneous flow over flat terrain. Here we represent the results corresponding to winds from west (from North sea, inhomogeneous terrain). There is no significant difference in the phase angles as compared with [5]. However, it is observed that the L and Γ parameters are significantly greater for the winds from west than those from east for the same height span as given in Table 2.

Table 2. L and Γ parameters at Høvsøre for the winds from east ([5]) and west.

Wind direction	L(m)	Γ
60° and 120°	40	3.3
240° and 300°	190	4.2

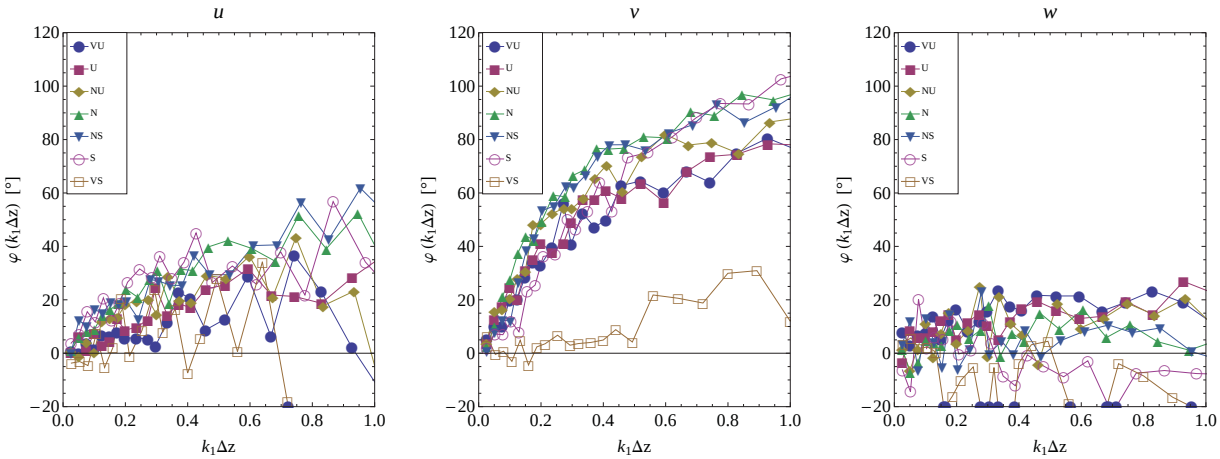

Figure 6. The phases between 40 and 100 m at Høvsøre for different atmospheric stabilities for wind directions between 60° and 120°. Atmospheric stability is classified into seven stabilities (very unstable to very stable) following [16].

It should be noted that the model spectra fits in Figure 3 are very poor because the upstream surface conditions are inhomogeneous, and that the fits from the eastern sector presented in Chougule et al. [5] are much better. The predicted coherences in Figure 4 (b) are correspondingly poor (again much worse than in Chougule et al. [5]), but the phases are still reasonable.

As discussed in Section 3.1, the phases from the Mann model are functions of L and Γ parameters. The model phases increase with the decrease in L parameter and increases with the increment in Γ. At a given mean wind speed (say 8 m s^{-1}), the turbulence length scale decrease from very unstable towards very stable (Ref. [4]) and hence the model phases should increase. However, as shown in [4] there is no systematic effect of atmospheric stability on Γ at a given mean wind speed. Following this discussion, it can be concluded that there is no systematic effect of atmospheric stability on the phase angles. This can also be seen from Figure 5. The stability based phase analysis is new relative to Chougule et al. [5]. However, the study in [4] is also restricted to winds at Høvsøre from east and the above discussion should make more sense when we observe the diabatic phase angles corresponding to winds from east as depicted in Figure 6. For the winds from west reader may able to find systematic decrease in v-phase from very unstable towards vary stable by observing Figure 5.

More intuitive explanation behind the behavior of the phase angles due to shear based on rapid distortion theory may be found in Chougule et al. [5].

6. Conclusions

The phase angles of all three velocity components are analysed from Høvsøre data for inhomogeneous terrain under diabatic conditions. These phases behave similarly to those under

neutral ABL with no significant changes. The diabatic phase angles from inhomogeneous flow are insignificantly different than those for homogeneous flow. There is no systematic effect of atmospheric stability on the phase angles. Phases of the cross-spectra of all three velocity components show systematic behaviour: $\varphi_v > \varphi_u > \varphi_w$ for $k_1\Delta z \leq 1$. RDT model is able to predict the observed neutral, inhomogeneous phase ordering.

Acknowledgements
This study is a part of the Ph.D. project funded by Siemens Wind Power A/S and WindScanner.dk which is funded by the Danish Agency for Science. We are also obliged to the COMWIND project funded by Danish Council of Strategic Research (DSF- contract: 09-067216).

References

[1] Tong C and Wyngaard J C 1996 *Bound.-Layer Meteorol.* **81** 105–121
[2] Mann J 1994 *J. Fluid Mech.* **273** 141–168
[3] Sathe A, Mann J, Gottschall J and Courtney M S 2011 *J. Atm. and Oce. Tech.* **28(7)** 853–868
[4] Sathe A, Mann J, Barlas T, Bierbooms W A A M and van Bussel G J W 2012 Influence of atmospheric stability on wind turbine loads (*Preprint* DOI: dx.doi.org/10.1002/we.1528)
[5] Chougule A, Mann J, Kelly M, Sun J, Lenschow D H and Patton E G 2012 *Journal of Turbulence* **13(36)** 1–13 (*Preprint* DOI:10.1080/14685248.2012.711524)
[6] Poulos G S, Blumen W, Fritts D C, Lundquist J K, Sun J, Burns S P, Nappo C, Banta R, Newsom R, Cuxart J, Terradellas E, Balsley B and Jensen M 2002 *Bull. Amer. Meteor. Soc.* **83** 555–581
[7] Sun J, Burns S P, Lenschow D H, Banta R, Newsom R, Coulter R, Fraiser S, Nappo C, Cuxart J, Blumen W, Lee X and Hu X Z 2002 *Bound.-Layer Meteorol.* **105** 199–219
[8] Heidrick T R, Banerjee S and Azad R S 1977 *J. Fluid Mech.* **81** 137–154
[9] Komori S, Ueda H, Ogino F and Mizushina T 1983 *J. Fluid Mech.* **130** 13–26
[10] Veers P S 1988 Three-dimensional wind simulation Tech. Rep. SAND88-0152 Sandia National Laboratories
[11] Veers P S 1984 Modeling stochastic wind loads on vertical axis wind turbines Tech. Rep. SAND88-1909 Sandia National Laboratories
[12] Mann J 1998 *Prob. Engng. Mech.* **13(4)** 269–282
[13] Pope S B 2000 *Turbulent Flows* 1st ed (UK: Cambridge University Press)
[14] Townsend A A 1976 *The structure of turbulent shear flow* 2nd ed (UK: Cambridge University Press)
[15] IEC 2005 Wind turbines part 1: Design requirements Tech. Rep. IEC 61400-1
[16] Gryning S, Batchvarova E, Brmmer B, Jrgensen H and Larsen S 2007 *Bound.-Layer Meteorol.* **124** 251–268
[17] Sun J, Lenschow D H, Burns S P, Banta R M, Newsom R K, Coulter R, Frasier S, Ince T, Nappo C, Balsley B B, Jensen M, Mahrt L, Miller D and kelly B S 2004 *Bound.-Layer Meteorol.* **110** 255–279
[18] Mann J 2000 *J. Wind Eng. and Ind. Aero.* **88** 153–169
[19] von Kármán T 1948 *Proc. Nat. Acad. Sci.* **34** 530–539
[20] Sullivan P P and Patton E G 2011 *J. Atmos. Sci.* **68** 2395–2415
[21] Brasseur J G and Wei T 2010 *Phys. Fluids* **22** 1–21